JOURNAL OF MAGNETIC RESONANCE **129,** 184–187 (1997)
ARTICLE NO. MN971258

Diffusion Imaging with Hyperpolarized ^{3}He Gas

David M. Schmidt,[1,]* John S. George,* Seppo I. Penttila,* Arvind Caprihan,† and Eiichi Fukushima†

*Los Alamos National Laboratory, Los Alamos, New Mexico 87545; and †Lovelace Respiratory Research Institute, 2425 Ridgecrest Dr. SE, Albuquerque, New Mexico 87108

Received March 12, 1997; revised July 25, 1997

We used MRI of hyperpolarized ^{3}He to demonstrate some novel aspects of gas diffusion. Two different techniques were used. First, a slice was burned into a one-dimensional image by inverting the spins in the slice and diffusion was studied by measuring the magnetization as it filled the depleted slice. A diffusion coefficient was determined by the fit of these data. Second, one-dimensional diffusion images were made using a Stejskal–Tanner PGSE method. This was done with and without a temperature gradient present, showing that the effect of temperature can be dynamically monitored by such diffusion images. © 1997 Academic Press

Several novel aspects of NMR or MRI with hyperpolarized noble gases have recently been demonstrated, including the ability to easily image gas-filled spaces (*1, 2*) and to transfer part of their polarization to other nuclei (*3, 4*). In this article we demonstrate some novel aspects of diffusion with MRI and hyperpolarized noble gases. We obtained one-dimensional images of ^{3}He gas diffusing into a slice marked by inversion of its magnetization, a technique previously used for observing diffusion of thermally polarized ^{129}Xe gas (*5*). Next the pulsed-gradient technique of Stejskal and Tanner (*6*) was used for making a one-dimensional diffusion image of the gas with and without a temperature gradient present. We have demonstrated that temperature changes can be dynamically monitored by diffusion images of ^{3}He gas.

The experiments were done in a NMR imager/spectrometer (Nalorac Cryogenics Corp.) with a 1.9-T, horizontal-bore, superconducting magnet (Oxford) having a bore diameter of 31 cm. The homogeneous region of the magnet allows a spherical volume of 8-cm diameter to be imaged. Rather than thermally polarizing the ^{3}He gas in the magnetic field of the imaging magnet, the gas was externally hyperpolarized through the technique of laser-optical pumping in the presence of rubidium molecules (*7, 8*). The ^{3}He gas was at 7 atm pressure in a cylindrical cell with inner dimensions 7.0 cm long and 2.2 cm in diameter. The portable polarizing apparatus was borrowed from a nuclear physics experiment and is described elsewhere (*9, 10*). For each set of images the gas was polarized in the fringe field of a 1.9-T magnet at a distance of 2 m for a few hours using a 15-W diode laser array (*11*). The polarization time constant of the cell (T_1) was about 15 h and with 4 h of optical pumping a polarization of about 5% was achieved. This is over 3 orders of magnitude greater than that which would be available from conventional thermal polarization and significantly improves the ability to image the gas. A two-dimensional projection image of the hyperpolarized gas is shown in Fig. 1.

A series of one-dimensional images over time was obtained in which the diffusion of two populations of nuclei could be seen in a manner similar to that of (*5*). First, the magnetization of nuclei in a thin central section of the cylinder was inverted. Then, images were taken every 0.2 s for a total of 5 s, using a constant flip angle of 4.5°. The series of images is shown in Fig. 2. These have been normalized to the same total intensity because a fraction ($\sin(4.5°)$) of the magnetization is lost with each image acquisition.

The ^{3}He diffusion coefficient was measured with these data using a simple model. A delta function spike in density will, through diffusion, form a density profile which is Gaussian whose variance is proportional to the diffusion coefficient and the time over which diffusion has taken place (*12*). We therefore modeled each one-dimensional image by convolving the first image with a Gaussian whose variance V was proportional to a candidate diffusion coefficient D times t, the time interval separating the two images: $V = 2Dt$. We then searched for the value of D which minimized the error between the predicted and measured values using the χ^2 statistic:

$$\chi^2(D) = \sum_{i,\tau} \left(\frac{x_{i,\tau} - \tilde{x}_{i,\tau}(D)}{\sigma_\tau} \right)^2. \qquad [1]$$

Here, $x_{i,\tau}$ is the value at pixel i in the image at time interval τ, $\tilde{x}_{i,\tau}(D)$ is the modeled value which depends on the diffusion coefficient, and σ_τ is the standard deviation of the noise for all the pixels in the image at time interval τ, estimated from the pixels outside those containing the gas cell. The model does not account for the cell boundaries so only pixels sufficiently far away from the boundaries as to not be affected

[1] To whom correspondence should be addressed at MS-D454, Los Alamos National Laboratory, Los Alamos, NM 87545.

1090-7807/97 $25.00

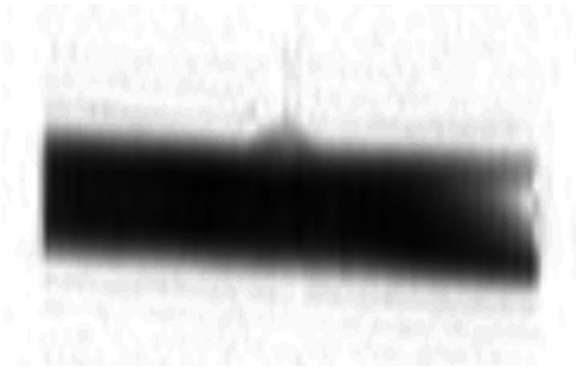

FIG. 1. A two-dimensional projection image of the hyperpolarized ^{3}He gas in its cylindrical cell. The small stem of about 1 mm in diameter used for filling the cell is visible in the top center portion of the image.

by them were used in the fit. In addition, to correct for the decreasing signal, each image was first normalized to the same total signal intensity. A comparison of the data to the modeled data with the best-fitting value of D is shown in Fig. 3 for a few selected time intervals. A value of $D = (21.3 \pm 0.4)$ mm^2/s was obtained.

The images of Fig. 2 show an asymmetry that is caused by having the inverted slice off-center so that there is more sample on one side of the slice than the other. Although the asymmetry at first sight is similar to that presented in (*13*), the B_0 field was perpendicular to the cylinder axis and the one-dimensional images are along the cylinder axis and perpendicular to B_0 for our case. Therefore, susceptibility-induced magnetic field inhomogeneities as discussed in (*13*) do not cause the asymmetry in our images.

Next, one-dimensional diffusion images were made using the technique of Stejskal and Tanner (*6*). A diffusion coefficient was calculated at each point in the image by taking the ratio of the image intensities with and without a previous magnetic field gradient in place. Atomic displacements in the presence of a magnetic field gradient will cause the signal to diminish. The experiment of Stejskal and Tanner (*6*) measures an effective diffusion coefficient D which is a measure of the atomic displacements between the two bipolar pulsed gradients. In the absence of barriers, the diffusive displacement is directly related to the usual definition of the diffusion coefficient.

The pulse sequence used for one-dimensional diffusion imaging is shown in Fig. 4. It is a gradient-echo sequence with an RF pulse of flip angle $\theta = 4.5°$ and bipolar gradient for diffusion measurement. The image intensity S at any position is given by

$$S = A \exp\left(-\gamma^2 D \int_0^T f^2(t)dt \right), \qquad [2]$$

where

$$f(t) = \int_0^t G_y(s)ds, \qquad [3]$$

and A is a scaling constant which includes the effects of the read-out gradient. For the trapezoidal-shaped gradient pulses

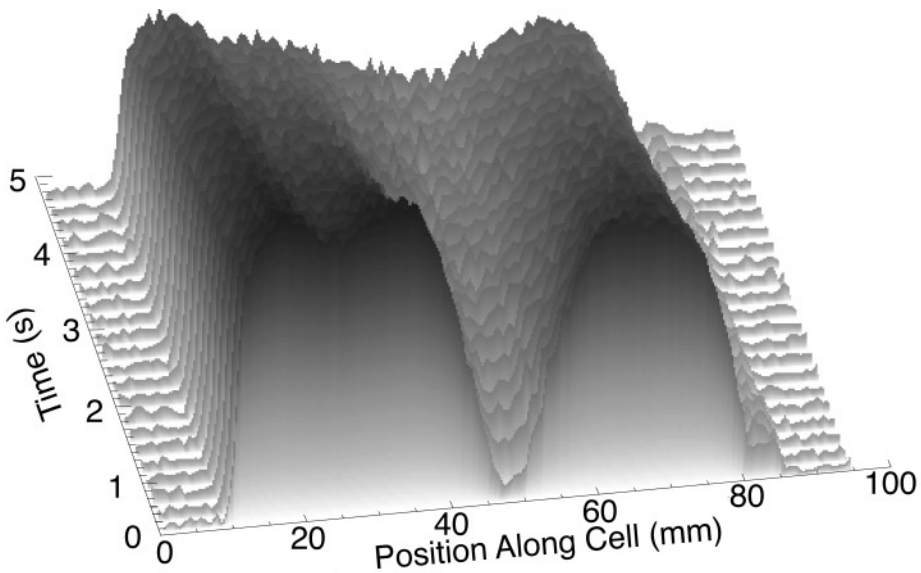

FIG. 2. A series of one-dimensional images of the gas over time, showing the diffusion of the small central slice of inverted magnetization. Time runs from front to back with the total duration being 5 s.

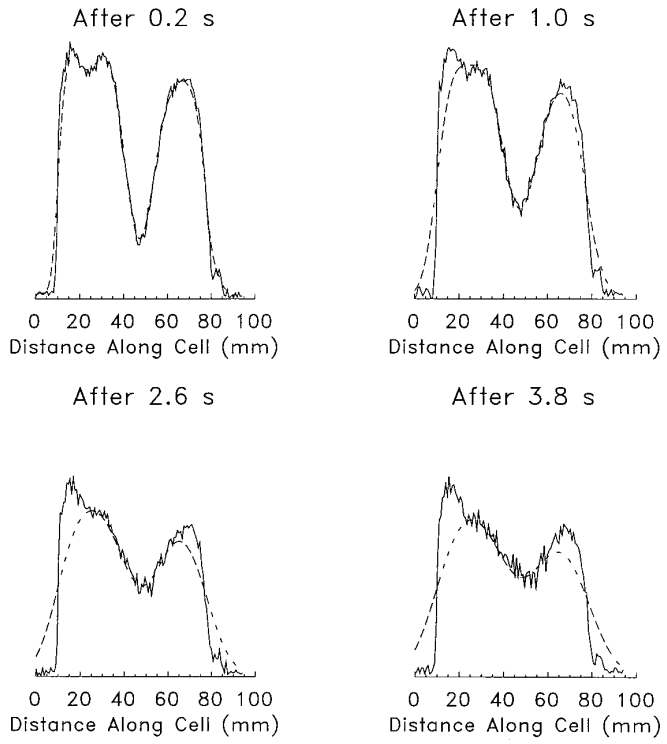

FIG. 3. A comparison of the data (solid lines) and model (dashed lines) for a few selected time intervals using the best-fit value of the diffusion coefficient. The model does not take into account the cell boundaries; only those pixels sufficiently far from the boundaries so as to not be affected are included in the fit.

$$\int_0^T f^2(t)dt = G^2[(L + R)^2(\Delta - L - 2R) + 2L^3/3 + 2L^2R + 23LR^2/6 + 23R^3/15]. \quad [4]$$

In our experiment the gradient pulses were adjacent to each other so that $\Delta = L + 2R$. With the gradient G measured in hertz per centimeter, $S \propto \exp(-\alpha D)$, where

$$\alpha = (2\pi G)^2(2L^3/3 + 2L^2R + 23LR^2/6 + 23R^3/15). \quad [5]$$

The experimental parameters were $R = 320\ \mu$s, $L = 200\ \mu$s, and $G = 21{,}712$ Hz/cm. The gradient was along the length of the cell. Knowing the strength and duration of the magnetic field gradient allows the diffusion coefficient to be determined.

Diffusion can be affected by physical boundaries as well as by temperature or pressure. Diffusion images were made both at thermal equilibrium (Fig. 5a) and with a thermal gradient (Fig. 5b) produced by holding the right end (as viewed in this figure) of the cell in a liquid nitrogen exhaust plume for a few minutes. The diffusion constant at each pixel was calculated using Eq. [2] from two images, one with a gradient of $G = 21{,}712$ Hz/cm and the other with the gradient absent. The value of every fifth pixel averaged with its four nearest neighbors is shown in Fig. 5. The plot on the left is with the gas at equilibrium at room temperature. Error bars in these plots were obtained by estimating the standard deviation of the noise from a region outside the cylinder. Error bars in Fig. 5a are larger than those in Fig. 5b because the data for Fig. 5a were obtained after a shorter polarization time and therefore had lower signal. The diffusion measured away from the ends of the cylinder is consistent with that measured from observing the diffusion of a section of inverted magnetization, described above. The plot on the right shows a diffusion image when the cylinder had a thermal gradient. We see that the diffusion coefficient decreases with temperature.

Near the walls the gas motion becomes restricted and the displacement of spins is reduced. In our experiment with $D = 21$ mm^2/s and $\Delta = 0.84$ ms, the diffusion length scale was $l_D = \sqrt{D\Delta} = 0.1$ mm (*14*), which is considerably smaller than the image resolution of 0.8 mm. Therefore these experiments should not show effects of restricted diffusion and the reduced value of the diffusion constant at points 5 mm near the walls cannot be explained by such wall effects.

We have presented two different experimental techniques which yielded the ^{3}He self-diffusion coefficient of $D_{33} = (21.3 \pm 0.4)$ mm^2/s at about 7 atm pressure and at room temperature. A previous NMR measurement (*15*) at 300 K and at 1 Torr yields a value of $D_{33} = (27.1 \pm 1.5)$ mm^2/s at 7 atm when scaled by a factor of 5320, assuming a linear pressure dependence. Many measurements of ^{3}He–^{4}He diffusion have been made at atmospheric pressure using techniques other than NMR, as summarized in (*16*). All of these agree with each other to within 3%. When corrected for isotopic mass dependence and for pressure dependence, as described in (*15*), these yield a value of $D_{33} = 28.0$ mm^2/s

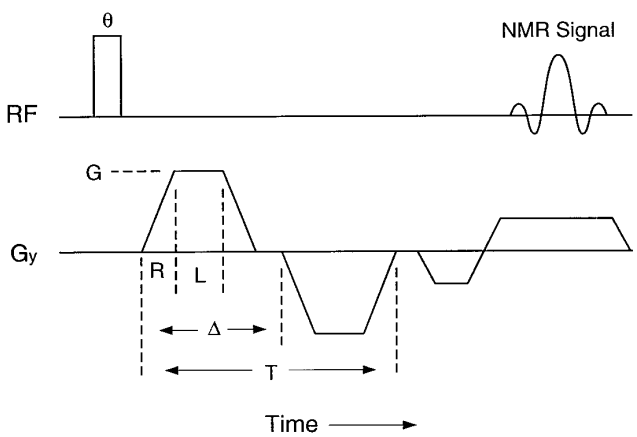

FIG. 4. The pulse sequence used for one-dimensional diffusion imaging of the cell. The gradient was along the length of the cell.

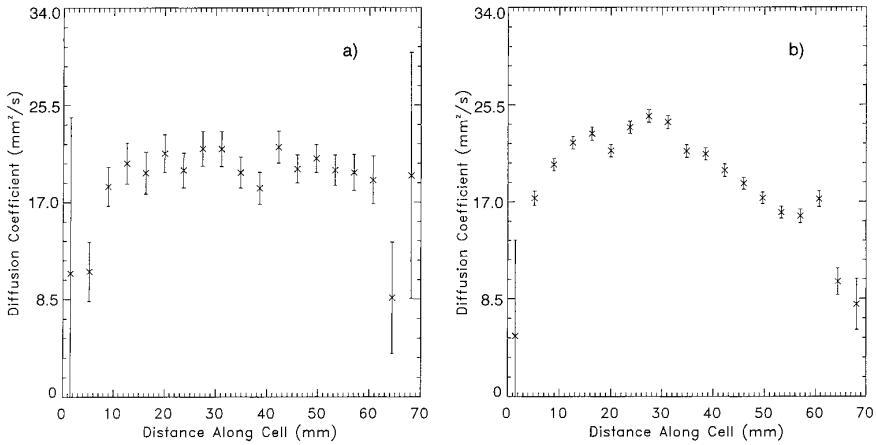

FIG. 5. Two diffusion images with (b) and without (a) a thermal gradient in place. The decrease in diffusion from left to right in the right-hand image reflects the decrease in temperature from left to right.

at 7 atm. Considering the type and scale of corrections needed to compare our results to previous results, the difference of about a factor of 2 may not be significant. Moreover, uncertainty of the pressure in our cell could account for this difference as well.

We have demonstrated the use of diffusion imaging with hyperpolarized noble gas for dynamically monitoring temperature and for detecting physical boundaries. Just like relaxation time images, spatial maps of diffusion can be another useful technique for characterizing the environment of the molecules containing the nuclei being imaged. We believe that diffusion imaging of hyperpolarized noble gases offers unique advantages in characterizing porosity of materials, studying fractures in rocks, and dynamically imaging pressure and temperature distributions in biological and acoustical systems.

REFERENCES

1. M. S. Albert, G. D. Cates, B. Driehuys, W. Happer, B. Saam, C. S. Springer, Jr., and A. Wishnia, *Nature* **370,** 199 (1994).
2. H. Middleton, R. D. Black, B. Saam, G. D. Cates, G. P. Cofer, B. Guenther, W. Happer, L. W. Hedlund, G. A. Johnson, K. Juban, and J. Swartz, *Magn. Reson. Med.* **33,** 271 (1995).
3. C. R. Bowers, H. W. Long, T. Pietrass, H. C. Gaede, and A. Pines, *Chem. Phys. Lett.* **205,** 168 (1993).
4. G. Navon, Y. Q. Song, T. Room, S. Appelt, R. E. Taylor, and A. Pines, *Science* **271,** 1848 (1996).
5. M. Pfeffer and O. Lutz, *J. Magn. Reson. A* **113,** 108 (1995).
6. E. O. Stejskal and J. E. Tanner, *J. Chem. Phys.* **42,** 288 (1965).
7. N. D. Bhaskar, W. Happer, and T. McClelland, *Phys. Rev. Lett.* **49,** 25 (1982).
8. W. Happer, E. Miron, S. Schaefer, D. Schreiber, W. A. van Wijngaarden, and X. Zeng, *Phys. Rev. A* **29,** 3092 (1984).
9. M. A. Espy *et al., Phys. Rev. Lett.* **76,** 3667 (1996).
10. B. Larson, O. Häusser, P. P. J. Delheij, D. M. Whittal, and D. Thiessen, *Phys. Rev. A* **44,** 3108 (1991).
11. W. Cummings *et al., Phys. Rev. A* **51,** 4842 (1995).
12. E. L. Cussler, ''Diffusion: Mass Transfer in Fluid Systems,'' p. 40, Cambridge Univ. Press, New York (1984).
13. B. Saam, N. Drukker, and W. Happer, *Chem. Phys. Lett.* **263,** 481 (1996).
14. P. T. Callaghan, A. Coy, L. C. Forde, and C. J. Rofe, *J. Magn. Reson. A* **101,** 347 (1993).
15. R. Barbé, M. Leduc, and F. Laloë, *J. Phys.* **35,** 935 (1974).
16. J. C. Liner and S. Weissman, *J. Chem. Phys.* **56,** 2288 (1972).